GENE DELIVERY

Journal of Controlled Release 143 (2010) 104–111

Contents lists available at ScienceDirect

Journal of Controlled Release

journal homepage: www.elsevier.com/locate/jconrel

Monitoring intracellular degradation of exogenous DNA using diffusion properties

Akira Sasaki, Masataka Kinjo *

Laboratory of Molecular Cell Dynamics, Faculty of Advanced Life Science, Hokkaido University, Kita21-Nishi11, Kita-ku, Sapporo, Hokkaido, 001-0021, Japan

ARTICLE INFO

Article history:
Received 30 September 2009
Accepted 16 December 2009
Available online 24 December 2009

Keywords:
Fluorescence correlation spectroscopy
Gene delivery
Exonuclease
DNA stability
Diffusion constant

ABSTRACT

Artificial nonviral gene vectors have the potential to improve the safety of gene therapy; however, such artificial vectors are less efficient for gene expression due to the existence of various barriers to delivery of exogenous DNAs to the nucleus in the living cell. Here we describe the degradation activities of cytoplasmic nucleases, which are involved as a barrier to efficient exogenous gene expression. The size and structure of degraded DNA were monitored by fluorescence correlation spectroscopy (FCS) and fluorescence cross-correlation spectroscopy (FCCS) in solution and in the cytoplasm of living cells. Differences in degradation by endo- and exonucleases were confirmed by differences in the size and structure of DNA. Moreover, we confirmed the influence of the exonuclease degradation in cytoplasm on the expression rate of DNA transfection with a cationic lipid. Based on a comparison of *in vitro* and cell measurements, we conclude that cytoplasmic degradation by exonucleases can be a considerable barrier against efficient gene delivery.

1. Introduction

Gene delivery systems with artificial nonviral vectors are widely used in the research field of cell biology and also in the clinical field as gene therapy to promote exogenous gene expression or inhibit production of a target protein. Nonviral vectors have advantages such as a low immune response and no risk of a disorder, which might be caused by native viral vector genome integration [1]. Therefore, for example, generation of induced pluripotent stem (iPS) cells with nonviral strategy has been studied [2]. However, nonviral vectors need to overcome the disadvantage of low gene expression efficiency compared with viral vectors [3]. In general, complexes of exogenous DNAs and a cationic polymer or cationic lipid, commonly used as nonviral vectors, are internalized to target cells by endocytosis. Then a sequential process progresses spontaneously with escape from endosomes, dissociation of complexes, and diffusion of naked DNAs in the cytoplasm to reach the nucleus [4–6]. On the other hand, physical approaches such as microinjection [7,8] and electroporation [9] are performed to incorporate naked DNAs directly into cytoplasm across the plasma membrane. Some naked DNAs diffuse in the cytoplasm to the nucleus [10]. The diffusion of exogenous DNAs in cytoplasm is relatively slow compared with that in solution [10,11], and it is hard for large DNA to cross the nuclear membrane [11]. Under such conditions in cytoplasm, the existence of nuclease degradation in cytoplasm is suggested [10–15]. It is presumed that the translocation and nuclear uptake of transfected DNA compete with degradation by cytoplasmic nucleases [11]. Therefore, it is important to investigate cytoplasmic behavior of naked exogenous DNAs to achieve efficient gene delivery and expression. The cytoplasmic degradation of naked DNAs can function as a barrier against efficient gene delivery. However, little is known about the degradation mechanism [13] because it is difficult to characterize the degradation process of exogenous DNA in living cells.

The purpose of this study was to investigate the mechanism of exogenous DNA degradation *in situ*, in cytoplasm, by analyses of diffusion properties of DNAs and to determine the effects of cytoplasmic degradation on the gene expression rate. Thus we employed FCS [10,16–18] to measure the diffusion properties of DNAs and FCCS [18–22] to monitor the degradation of DNAs by cytoplasmic nucleases at the single molecule level. Furthermore, we predicted that exonucleases would work as the main barrier in cytoplasm, so a capped structure was attached to the transfected DNA to enhance the expression of the protein EGFP.

In this work we describe the degradation mechanisms of cytoplasmic nucleases, which function as a barrier to efficient exogenous gene expression.

2. Material and methods

2.1. Double-fluorescent DNAs labeled by RG and Cy5

Rhodamine green (RG)- and Cy5-labeled DNAs were synthesized by PCR. PCR was performed with TaKaRa Ex Taq (Takara Bio Inc., Shiga, Japan) (5 U μl^{-1}), dNTP Mixture (0.2 mM each), Lambda-DNA (0.002 $\mu g\ ml^{-1}$) as a template, using a 5′-RG-labeled forward primer

Abbreviations: FCS, fluorescence correlation spectroscopy; FCCS, fluorescence cross-correlation spectroscopy; LSM, laser scanning microscopy; RG, rhodamine green.

* Corresponding author. Tel.: +81 11 706 9005; fax: +81 11 706 9006.
E-mail address: kinjo@sci.hokudai.ac.jp (M. Kinjo).

0168-3659/$ – see front matter © 2009 Elsevier B.V. All rights reserved.
doi:10.1016/j.jconrel.2009.12.013

and 5′-Cy5-labeled reverse primer (0.4 μM each; Sigma-Aldrich Japan, Tokyo, Japan). The sequences of primers used were:

forward primer: RG-5′-GAT GAG TTC GTG TCC GTA CAA CT-3′
reverse primer (for 100 bp): Cy5-5′-AGA CGG GCA ATC AGT TCA TCT TTC-3′
(for 200 bp): Cy5-5′-GTC ATC AAG CTC CTC TTT CAG CT-3′
(for 500 bp): Cy5-5′-GGT TAT CGA AAT CAG CCA CAG CG-3′
(for 23 bp annealing): Cy5-5′-AGT TGT ACG GAC ACG AAC TCA TC-3′

PCR products were purified 3 times using MicroSpin S-300 HR or S-400 HR columns (GE Healthcare, Waukesha, WI, USA). RG-23 bp–Cy5 was prepared by annealing of RG-labeled forward primer oligonucleotides with Cy5-labeled oligonucleotides that had the complementary sequence. The annealed product was treated with exonuclease I (10 U μg^{-1}; Takara Bio Inc., Shiga, Japan) and purified 3 times with G-25 columns (GE Healthcare, Waukesha, WI, USA).

2.2. Confocal imaging and fluorescence correlation spectroscopy

LSM and F(C)CS were carried out with a combination system consisting of an LSM510 and a ConfoCor2 (Zeiss, Jena, Germany) with a temperature control system (Fig. 1 and Supplementary Fig. S1). Rhodamine green and EGFP were excited by a 488 nm Ar-ion laser and Cy5 was excited by a 633 nm He–Ne laser through a water immersion objective (C-Apochromat, 40×, 1.2 NA; Zeiss, Jena, Germany). Emission signals were collected at 505–550 nm for RG or EGFP (green channel) and >650 nm for Cy5 (red channel) with avalanche photodiodes (APD). FCS and FCCS measurements were performed for 15–30 s three times.

The fluorescence autocorrelation functions of the red and green channels, $G_r(\tau)$ and $G_g(\tau)$, and the fluorescence cross-correlation function, $G_c(\tau)$, are calculated by

$$G_x(\tau) = \frac{\langle I_i(t) \cdot I_j(t+\tau) \rangle}{\langle I_i(t) \rangle \langle I_j(t) \rangle} \quad (1)$$

where τ denotes the time delay, I_i is the fluorescence intensity of the red channel ($i=r$) or green channel ($i=g$), $G_r(\tau)$ and $G_g(\tau)$ denote the autocorrelation functions of red ($i=j=x=r$), and green ($i=j=x=g$), or $G_c(\tau)$ denotes cross-correlation function ($i=r$, $j=g$, and $x=c$).

2.3. Distribution analysis by CONTIN algorithm

The distribution histogram of diffusion times was constructed using the CONTIN algorithm [23–26]. Instead of evaluating discrete diffusion processes with distinct species and their characteristic diffusion times (τD_i), the dynamic motion of DNAs in the cell can be distributed with regard to their diffusion times using the distribution

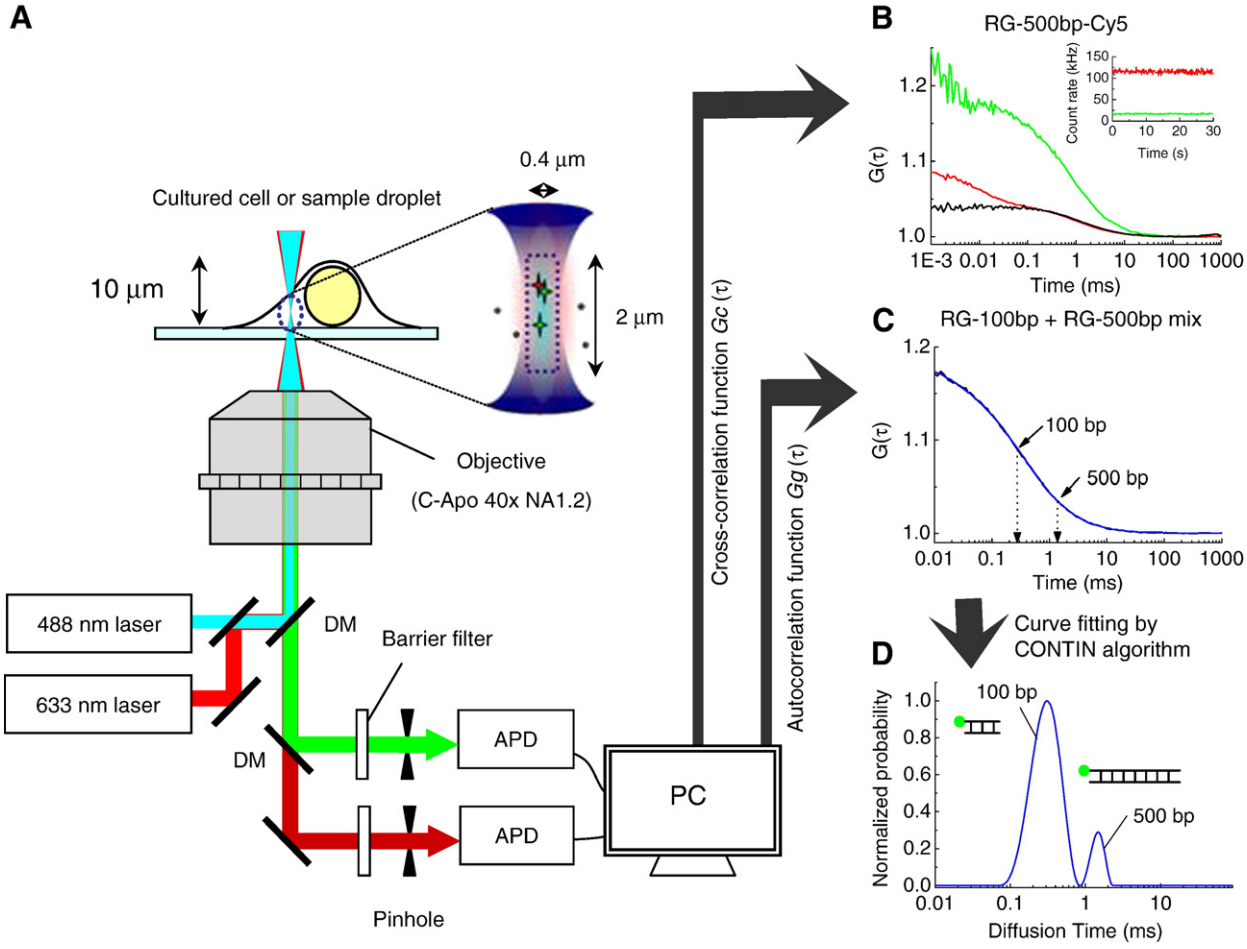

Fig. 1. Experimental setup for FCS and FCCS. (A) Diagram of microscope setup. DM: Dichroic mirror (B) Autocorrelation curves and cross-correlation curves of RG-500 bp–Cy5 obtained by FCCS measurement. (C) Autocorrelation curve of a mixture of RG-100 bp and RG-500 bp. (D) Distributions of diffusion times calculated from the autocorrelation curve using the CONTIN algorithm.

function $P(\tau D_i)$. The diffusion time (τD_i) corresponds to the average time for diffusion of fluorescent particles across the detection area, which reflects the size of particles. We analyzed $G(\tau)$, representing the distribution of diffusion times according to the expression of multiple components:

$$G(\tau) = 1 + \frac{1}{N}\left\{1 - f\left(f\exp\left(\frac{-\tau}{\tau_t}\right)\right)\right\}\int_i P(\tau D_i)\left(1+\frac{\tau}{\tau D_i}\right)^{-1} \times\left(1+\frac{\tau}{s^2\tau D_i}\right)^{-1/2} d\tau D_i \quad (2)$$

where N represents the average number of fluorescent particles in the detection volume defined by radius ω and length $2z$, and s is the structural parameter representing the ratio $s = z/\omega$. The value of f is the average fraction of molecules in the triplet state. The value of τ_t is the triplet state decay time. The values of f and τ_t were fixed to $f = 0.1$ and $\tau_t = 0.02$ ms in the analyses.

2.4. Enzyme degradation tests in solution

DNA solution was incubated with 0.02 U μl^{-1} of exonuclease III (Takara Bio Inc., Shiga, Japan), 0.0001 U μl^{-1} of DNase I (Takara Bio Inc., Shiga, Japan) or 0.001 U μl^{-1} of the BAL31 nuclease (Takara Bio Inc., Shiga, Japan) in a total volume of 50 μl. The incubation was performed at 37 °C on the microscope stage. FCS and FCCS measurements were carried out 8 times in 84 or 97 min.

2.5. Cell culture

Cells were maintained in a 5% CO_2 humidified atmosphere at 37 °C in Dulbecco's modified Eagle's medium (DMEM, Sigma, St. Louis, MO, USA) supplemented with 10% fetal bovine serum (Invitrogen, Carlsbad, CA, USA), 1×10^5 U l^{-1} penicillin G and 100 mg l^{-1} streptomycin sulfate. The day before transient transfection, cells were plated on a 35-mm glass-base dish (AGC Techno Glass, Ltd., Chiba, Japan) or 6-well plate (Nalge Nunc International, Naperville, IL, USA) to 60–70% confluence in each well. Dishes for HEK293 cells were treated with Cellmatrix Type I-C (Nitta Gelatin Inc., Osaka, Japan). The medium was replaced by phenol red-free medium (Opti-MEM, Invitrogen, Carlsbad, CA, USA) before confocal imaging.

2.6. Bead-loading method

Acid washed beads (~106 μm; Sigma-Aldrich, St. Louis, MO, USA) were siliconized in a closed chamber by dimethyldichlorosilane (Sigmacoat SL-2; Sigma-Aldrich, St. Louis, MO, USA) for 1 h at room temperature and then autoclaved. Before DNA loading, the medium was removed, and 10 μl of DNA (3 μg μl^{-1}) was placed on the cells cultured on glass-base dishes. The cells were then covered with 100 μl of dried glass beads, tapped vertically 3–5 times, and immediately rinsed with Opti-MEM to remove the beads [27,28].

2.7. Construction of end-capped DNAs

Linear DNAs (1.6–4 kbp) that had restriction sites of EcoR I and Pst I at DNA ends were synthesized by PCR using plasmid pEGFP-C1 (Clontech, Palo Alto, CA, USA), with deleted EcoR I and Pst I restriction sites in the multicloning site as a template. The sequences of primer sets used were:

(for 1572 bp): 5′-GGA CGA ATT CCG CCA TGC ATT AGT TAT TAA-3′
5′-GGA CCT GCA GGG ACA AAC CAC AAC TAG AAT-3′
(for 1972 bp): 5′-GGA CGA ATT CAA CGC CTG GTA TCT TTA TAG-3′
5′-GGA CCT GCA GCC ACG TTC TTT AAT AGT GGA-3′
(for 2972 bp): 5′-GGA CGA ATT CGA TCT TCT TGA GAT CCT TTT-3′
5′-GGA CCT GCA GTT TGC ATA CTT CTG CCT GCT-3′
(for 3972 bp): 5′-GGA CGA ATT CAA TCG TTT TCC GGG ACG CCG-3′
5′-GGA CCT GCA GGC TGC CTC GTC TTG CAG TTC-3′

Double digestion with EcoR I and Pst I (1 U each μg^{-1} of DNA; Takara Bio Inc., Shiga, Japan) was performed at 37 °C for 6 h. Oligonucleotides with 5′ phosphorylation were purchased from Sigma-Aldrich Japan (Tokyo, Japan):

(for EcoR I) 5′-AAT TTG TCC GCG TTG GCT TTT GCC AAC GCG GAC A-3′
(for Pst I) 5′-CTA CCT TGC GAG CTT TTG CTC GCA AGG TAG TGC A-3′.

Before ligation, the hairpin form of the oligonucleotide presenting a sticky end was obtained by boiling and subsequently cooling the sample in ice. Ligation of the fragment with the oligonucleotide cap was performed overnight at 16 °C with a 15-fold molar excess of each oligonucleotide and T4 DNA ligase (10 U μg^{-1} of DNA; Takara Bio Inc., Shiga, Japan).

The excess oligonucleotides and the uncapped fragments were digested by exonuclease III (10 U μg^{-1} of DNA) and exonuclease I (10 U μg^{-1} of DNA) at 37 °C for 15 h. Digested fragments and dimers of hairpin oligonucleotides were removed by isopropanol precipitation and a MicroSpin S-400HR column.

2.8. Expression assay

Cells in 6-well plates were transfected using Lipofectamine2000 (Invitrogen, Carlsbad, CA, USA) with 1 μg of DNA per well according to the manufacturer's instructions. The culture medium was discarded and the cell lysate harvested after incubation of cells for 10 min at room temperature in 200 μl of CelLytics-M (Sigma, St. Louis, MO, USA). The lysate was centrifuged for 10 min at 15,000 g at 4 °C. The EGFP gene expression rate was quantified by FCS measurements with 50 μl of supernatant. The expression efficiency was calculated as the ratio of the EGFP expression rate of transfected DNA (E) to the rate of the pEGFP-C1 plasmid (E_p) by the following equation:

$$\text{Expression efficiency} = E \Big/ E_p = \frac{N\cdot M / W}{N_p\cdot M_p / W_p} \quad (3)$$

where N, W, and M represent the number of EGFPs obtained from FCS measurement, the transfected DNA weight and molecular weight of transfected DNA, respectively. N_p, W_p and M_p represent the values with the pEGFP-C1 plasmid as a reference. We compared the expression efficiency values of each capped or uncapped DNA pair by using Student's t test to determine whether their means were significantly different.

3. Results

3.1. Diffusion analysis of constructed DNAs in solution

A series of linear DNAs from 23 bp to 500 bp that were labeled with rhodamine green (RG) and Cy5 on both 5′ ends (RG-DNA–Cy5) were synthesized by PCR. The size and purity of the linear DNAs were confirmed by agarose gel electrophoresis with SYBR Gold stain (Fig. 2A). Autocorrelation curves of the green fluorescence channel ($G_g(\tau)$) and red fluorescence channel ($G_r(\tau)$), and a cross-correlation curve ($G_c(\tau)$) were obtained by FCCS measurements of RG-DNA–Cy5 in solution. To assess the degree of cross-correlation amplitude, relative cross-correlation amplitude (RCA) was calculated by dividing $G_c(0) - 1$ by $G_r(0) - 1$ (for details, see Supplementary methods online). The RCA value was 0.908 ± 0.020 (mean ± S.D.) for the 500 bp DNA, which had double-fluorescent labels (Fig. 2B, the other cross-correlation curves are shown in Supplementary Fig. S2), and 0.104 ± 0.023 for the mixture of fluorescent primers that were used in the PCR reactions (Fig. 2C). The RCA value represents the fraction of DNAs that have RG and Cy5 fluorophores at both DNA ends, thus intact DNAs.

To extract information concerning the relative abundance and length of the DNA from the autocorrelation curve, we used the CONTIN algorithm [23–26]. The algorithm can determine the distribution of the correlation time with multiple peaks and its probability without any prior assumption about the number of peaks. Fig. 2D shows the distributions of diffusion times that were calculated from the autocorrelation curve of the green channel by using the CONTIN algorithm. The spectra of diffusion times of RG-DNA–Cy5 were separated from each other. This result suggested that the length of the DNA could be estimated with sufficient resolution in this range.

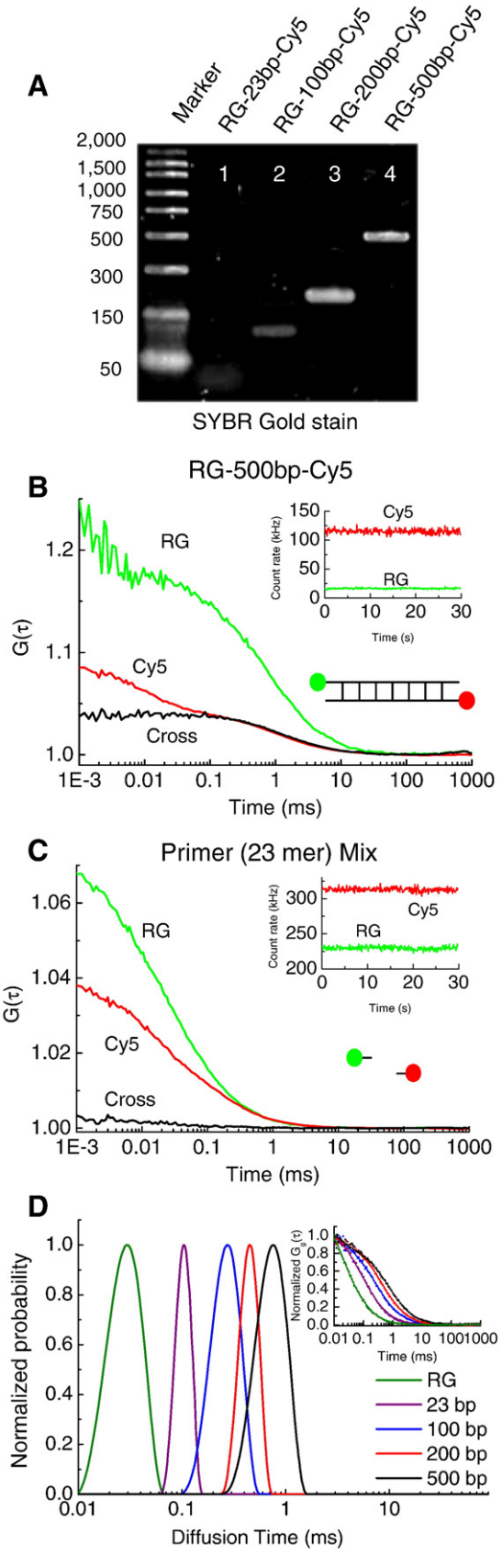

Fig. 2. Characterization of double-fluorescent-labeled DNAs in solution. (A) Agarose gel electrophoresis (2.5%) of PCR-synthesized DNA fragments. DNA was stained with SYBR Gold. (B) Auto- and cross-correlation curves of RG-500 bp–Cy5 DNA in 10 mM Tris–HCl (pH 7.4). (Insets) The fluorescence intensities in the red and green channels during FCCS measurement. RG, Cy5 and Cross represent $G_g(\tau)$, $G_r(\tau)$ and $G_c(\tau)$, respectively. (C) Auto- and cross-correlation curves of a mixture of RG-primer and Cy5-primer (23 mer each) as a negative control. (D) Distributions of diffusion times $P(\tau D_i)$ of various sizes of RG-DNA–Cy5 calculated from autocorrelation curves of the green channel by CONTIN algorithm. (Inset) Normalized autocorrelation curves $G_g(\tau)/G_g(0)$ (dot) with fitted curves (line) of DNAs in 10 mM Tris–HCl (pH 7.4) at room temperature.

3.2. Enzymatic degradation analysis in solution

To confirm whether FCS and FCCS could identify the degradation mechanisms of different nucleases, we monitored the DNA degradation with DNase I (an endonuclease that acts randomly), exonuclease III (an exonuclease that acts in the 3′ to 5′ direction) and BAL31 nuclease (an exonuclease that acts in both 5′ to 3′ and 3′ to 5′ directions) in solution. The nucleases were added to RG-500 bp–Cy5 solution in a droplet on a coverslip and FCCS measurements were performed as a function of time.

Fig. 3A, B and C shows the RCA changes of cross-correlation curves (Supplementary Fig. S3) of RG-500 bp–Cy5 with the three nucleases. With DNase I and BAL31 nuclease, RCA values rapidly decreased after the nuclease addition. In contrast, with exonuclease III, the RCA value did not decrease until 11 min. This indicated that the fluorophores did not separate in the initial phase of degradation (Fig. 3B insets). The RCA value was not changed without addition of a nuclease in the measurement time (Supplementary Fig. S4). We regarded 11 min as the initial phase, 31 min as the transient phase and 84–97 min as the stable phase of enzymatic reaction in Fig. 3A, B and C. We performed CONTIN analysis and compared distributions of diffusion times in each phase (Fig. 3D–L). The distribution peak became wider and shifted to the left with addition of DNase I (Fig. 3D, G and J). The peak width reflects the various lengths of DNA fragments generated by DNase I random degradation. In the case of exonuclease III, the enzyme generates two kinds of single-stranded DNA with the same sizes as the final products. The diffusion time shifted to the left at 31 min after nuclease addition without widening of the peak (Fig. 3E, H and K). Interestingly, two distribution peaks were detected with the BAL31 nuclease. A faster peak of diffusion times represents small fragments of DNA, with a level of diffusion time comparable to that of the RG fluorophore and a slower peak represents intact DNA. This result is reasonable since the BAL31 nuclease degrades the DNA from both the 5′ and 3′ ends where the fluorophore is attached. Thus, we could identify the different enzymatic behaviors by using FCCS and distribution analysis of FCS without any separation method such as gel electrophoresis or gel filtration.

3.3. Detection of diffusion properties of exogenous DNAs in cytoplasm

To classify nuclease activity in the cytoplasm of living cells, fluorescent-labeled DNAs were directly introduced into the cytoplasm of COS7 cells by the bead-loading method [27,28]. RG-100 bp–Cy5 did not enter freely into the nucleus (Fig. 4A inset and Supplementary Fig. S5), though RG-23 bp–Cy5 localized strongly in the nucleus (Supplementary Figs. S5 and S6).

Auto- and cross-correlation curves of RG-100 bp–Cy5 were obtained at the crosshair point in the laser scanning microscopy (LSM) image of the living cell in which DNAs were incorporated into the cytoplasm. High cross-correlation amplitude was detected within

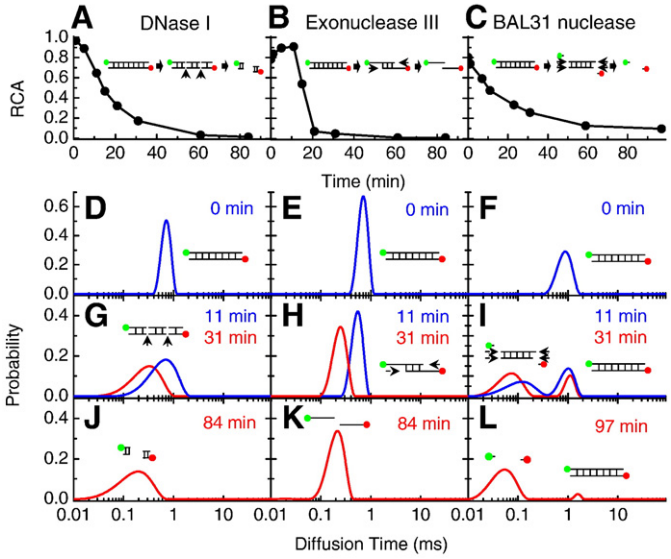

Fig. 3. Real-time monitoring of DNA degradation in 50 μl DNA solutions. Relative cross-correlation amplitudes, $(G_c(0)-1)/(G_r(0)-1)$ after addition of (A) 0.0001 U μl^{-1} DNase I, (B) 0.02 U μl^{-1} exonuclease III, and (C) 0.001 U μl^{-1} BAL31 nuclease. Distributions of diffusion times $P(\tau D_i)$ calculated by CONTIN algorithm from $G_g(\tau)$ at several time points after the addition of DNase I (D, G, J), exonuclease III (E, H, K) and BAL31 nuclease (F, I, L).

10 min after loading (Fig. 4A). However, cross-correlation amplitude was reduced after 45-min incubation at 37 °C in the same cell (Fig. 4B). This reduction indicated that exogenous DNA was degraded in cytoplasm. DNA diffusion properties were also analyzed by distributions of diffusion times using the CONTIN algorithm. At 45 min after introduction, a faster peak (around 0.2 ms) appeared in distributions of diffusion times (Fig. 4D).

To determine the origin of each peak in the distributions of diffusion times, autocorrelation curves $G_g(\tau)$s (Supplementary Fig. S7) of different DNA sizes that were obtained for the cytoplasm of HeLa cells were averaged ($N=4$–8) and analyzed using the CONTIN algorithm (Fig. 5). Two peaks of diffusion times were detected in each measurement; faster peaks were of the same order of diffusion time as the free RG fluorophore. On the other hand, the diffusion times of the slower peaks shifted to the right according to the increase in size of incorporated DNA (Fig. 5A, B and C). The diffusion times of DNAs in cytoplasm were 5–10 times slower than those in solution. This ratio was in good agreement with the previously reported value [9] and this result agreed well with the 5′ to 3′ exonuclease degradation models in solution (Fig. 3F, I and L). Finally, the appearance of 5′ to 3′ exonuclease activity was identified in cytoplasm by direct observations of incorporated exogenous DNAs using the distribution pattern of diffusion times.

3.4. Effect of DNA end-capping on the EGFP expression efficiency

To confirm the enzymatic activity of the 5′ to 3′ exonuclease in cytoplasm, we carried out an inhibition experiment for the enzyme using end-capped DNAs and monitoring the expression rate of EGFP. If exonuclease degradation works as a barrier against DNA transfection, the use of longer DNA and/or end-capped-DNA that protects the coding regions from each terminal (Fig. 6A) should increase the expression efficiency.

We synthesized linear DNAs of various lengths that were capped on both DNA ends by a hairpin-shape oligonucleotide [29,30]. Fig. 6B shows the analysis of the stability of a PCR-synthesized 2 kbp DNA and the end-capped DNA by agarose gel electrophoresis. The end-capped DNA remained intact after incubation with exonuclease III. This result

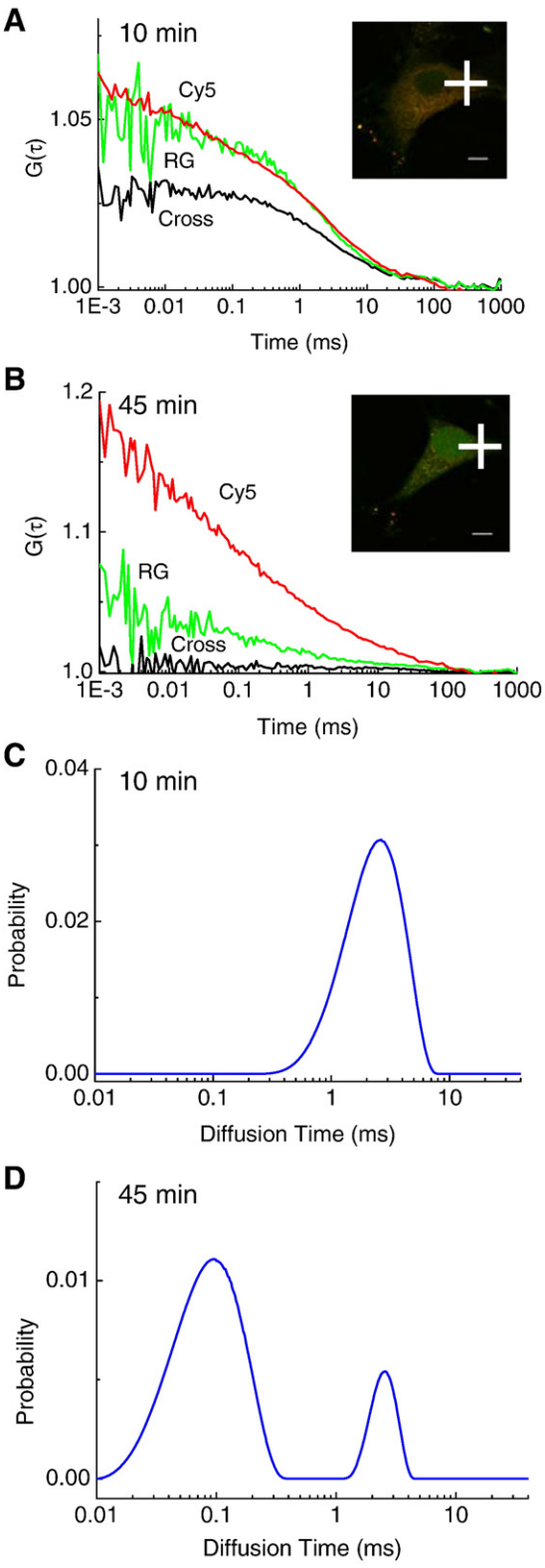

Fig. 4. Nuclease degradation of double-fluorescent-labeled DNAs in cytoplasm of a living COS7 cell. Auto- and cross-correlation curves of RG-100 bp–Cy5 DNA (A) 10 min and (B) 45 min after loading of DNAs in the same cell. FCCS measurements were carried out at the crosshairs in each laser scanning microscopy (LSM) image (insets). Scale bar represents 10 μm. RG, Cy5 and Cross represent $G_g(\tau)$, $G_r(\tau)$ and $G_c(\tau)$, respectively. Distributions of diffusion times $P(\tau D_i)$ of DNAs calculated by CONTIN algorithm from (C) $G_g(\tau)$ in panels A and (D) $G_g(\tau)$ in panel B.

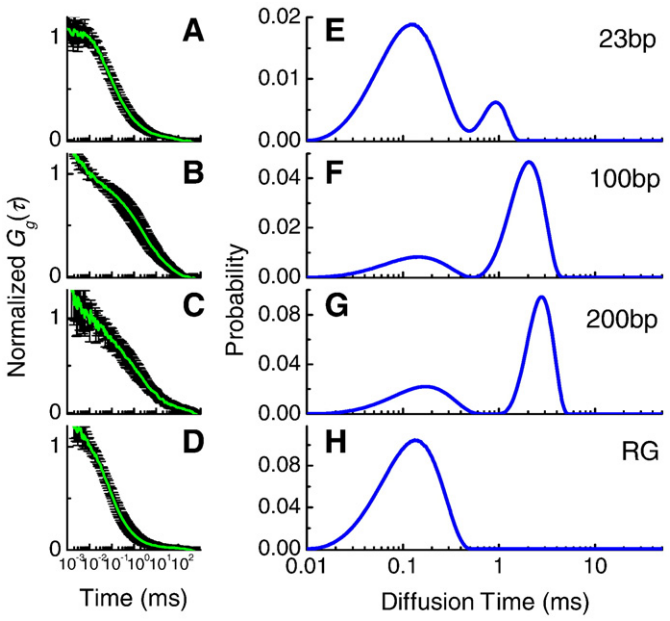

Fig. 5. Relationship between DNA size and diffusion time in living HeLa cells. The average of $G_g(\tau)$ curves in HeLa cytoplasm at 30 min after (A) RG-23 bp–Cy5 (B) RG-100 bp–Cy5 (C) RG-200 bp–Cy5 loading. (E–G) Distributions of diffusion times $P(\tau D_i)$ of DNAs calculated from the average of $G_g(\tau)$ curves using CONTIN algorithm. RG dye was also tested as a reference (D, H). Averaged correlation curves are expressed as the mean ± S.D. of 4–8 different experiments.

showed that end-capped DNA was resistant to degradation by exonuclease III. Fig. 6C, D, E and F shows the expression efficiencies of DNAs in HeLa, COS7, MEF and HEK293 cells, respectively. The expression efficiency was based on the EGFP expression per copy of transfected DNA (more details in Material and methods section).

Expression efficiencies of short DNAs such as that with a 1.6 kbp length were lower than those of other lengths in each cell line. When the expression efficiencies of non-capped PCR products and capped DNAs were compared, it was clear that DNA capping significantly increased the expression efficiency of 4 kbp DNA in HeLa, COS7 and MEF cells. However, the end-capping did not enhance the expression rate for short DNA lengths. In MEF cells, uncapped DNAs of all lengths were little expressed and capped DNAs exhibited ~10-fold greater gene expression than the uncapped DNAs. The effect of DNA capping was not observed in HEK293 cells. Although there were differences in the cell lines, the results obtained for HeLa, COS7 and MEF cells confirmed the effect of exonuclease degradation on DNA transfection.

4. Discussion

Our goal is to control the exogenous gene expression in nonviral gene therapy. Here we propose a new concept of nuclease characterization by monitoring the degradation patterns of oligonucleotides based on the fragment size and direction of degradation in living cells. The concept is conventional in that it is carried out using radioisotope-labeled oligonucleotides and a separation procedure such as gel electrophoresis to determine molecular size and distribution. The relationship between the exogenous DNA expression level and DNA stability by extension of DNA

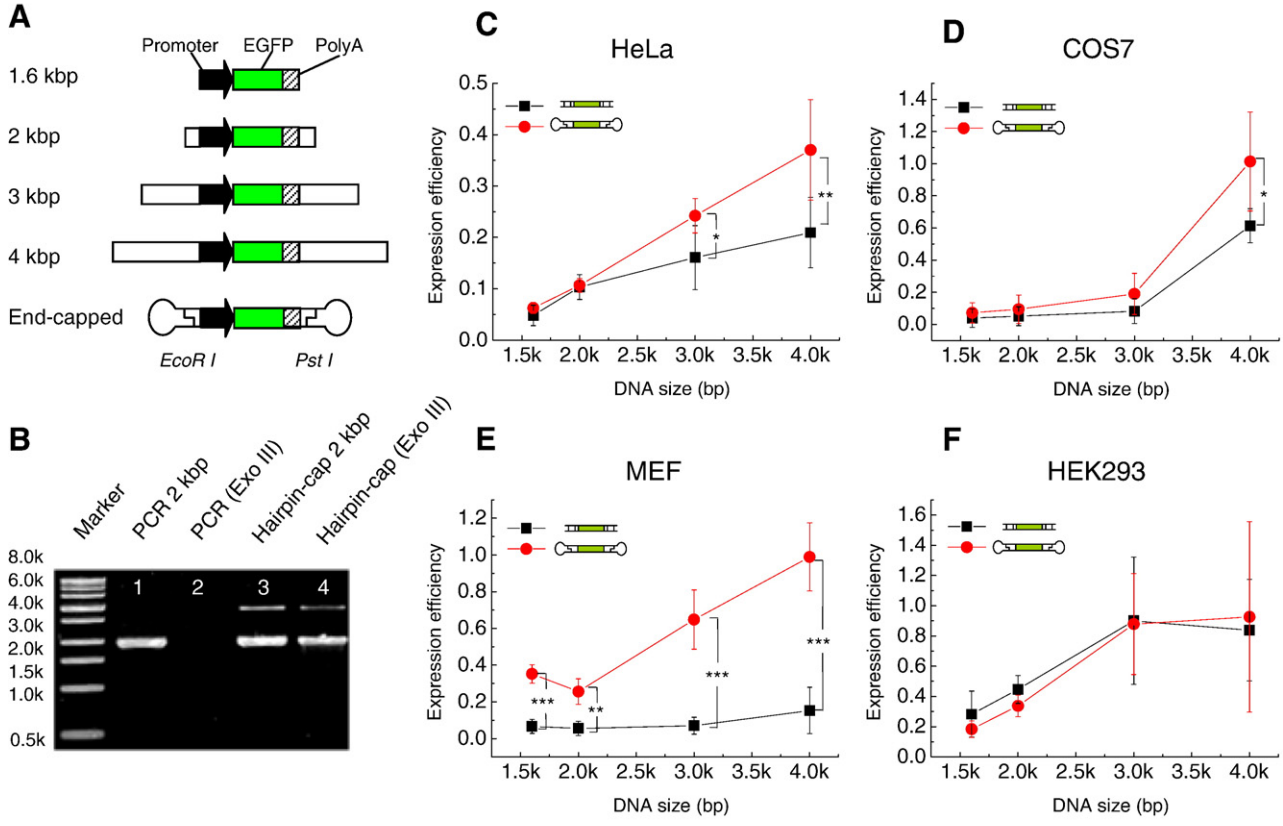

Fig. 6. Effect of DNA protection against exonucleases on expression efficiency with a cationic lipid. (A) Schematic diagram of various sizes of DNA expressing EGFP and end-capped DNA. (B) Agarose gel electrophoresis of uncapped and capped 2 kbp DNA (lanes 1 and 3). DNAs were incubated for 3 h at 37 °C in the presence of exonuclease III (lanes 2 and 4). (C) HeLa, (D) COS7, (E) MEF and (F) HEK293 cells were transfected with 1 μg of uncapped or capped linear DNA per well. Complexes were formed with Lipofectamine2000 reagent. Expression efficiency (E/E_p) is expressed as the mean ± S.D. of 4–5 different experiments. To normalize the values from each individual experiment, the expression rate of DNA (E) was divided by the rate using the pEGFP-C1 plasmid (E_p). *, $P<0.05$; **, $P<0.01$; ***, $P<0.001$ (Student's t test). Black symbols, uncapped DNA; red symbols, capped DNA.

fragments was studied using the luciferase assay *in vitro* and *in vivo* [31]; however, this assay in a cell homogenate only provides information on bulk DNA stability, not on the individual DNA degradation mechanism. Our approach is, therefore, replacement of the conventional concept by diffusion measurement using a fluorescent tag and coincident analysis using FCS and FCCS so that sensitivity is enhanced to the single molecule level and a physical separation procedure is not needed. Therefore, our method can be employed for measurements in single living cells.

DNA degradation in living cells has been studied based on the disappearance of fluorescent intensity in microscopic images of cells [14]. However, this method could not distinguish enzyme activity, from translocation and quenching. We employed FCCS to discriminate the intact DNA from degraded DNA fragments at the single molecule level with constant fluorescence intensity.

Furthermore, distribution analysis of diffusion times using CONTIN algorithm clearly showed different peak patterns for different enzymatic activities. The distributions of diffusion times had two peaks in cytoplasm. The diffusion time of the faster peak was almost the same as that of fluorescent dye alone, whereas the other, slower peak depended on the size of the DNA that was incorporated. Moreover, moderately sized DNA fragments were not detected in the cytoplasm. Taken together, these findings helped us to determine that (i) how, (ii) when, and (iii) where incorporated DNAs were degraded in the living cell. (i) The main mechanism of exogenous DNA degradation in cytoplasm was 5′ to 3′ exonuclease activity rather than endonucleases. (ii) The time scale of degradation (<45 min) was determined by real-time measurement without invasive treatment. (iii) The location of DNA degradation was not in small compartments but in cytoplasm because the monitored DNAs were distributed homogenously and had free diffusion values.

Finally, we confirmed the influence of the exonuclease degradation in cytoplasm on the expression rate of DNA transfection with a cationic lipid. The nuclease activity was inhibited by capped structures on the 3′ and 5′ ends of the DNA.

Interestingly, the end-capping effect on the expression rate was different in the cell lines.

In MEF cells, which are generally said to be hard to transfect [32], the end-capping effect was significant (Fig. 6E). On the other hand, in HEK293 cells, which are generally used in transfection assays because of their high expression efficiency [33–35], no end-capping effect was observed (Fig. 6F). These results agreed with previous reports that the transfected plasmids were more stable in HEK293 cells than in COS, NIH-3T3, HeLa [36].

In summary, our results show that exonuclease activity is related to transfection efficiency, though the level of exonuclease activity in cytoplasm might be different depending on the cell line.

To our knowledge, this is the first study that directly demonstrates the cytoplasmic degradation of exogenous DNAs using FCCS. It should be noted that the DNA diffusion was no longer monitored after fluorescent-labeled nucleotides were released from DNAs by exonucleases, so the method could not determine the full enzyme activity. On the other hand, a DNA full-labeling procedure such as single molecular DNA sequencing can resolve this drawback [37].

5. Conclusions

We clearly determined the DNA degradation mechanism, 5′ to 3′ exonuclease, in cytoplasm by measuring DNA diffusion properties at the single molecule level. Our method using noninvasive monitoring of the diffusion properties of DNA provides information on the fate of intracellular exogenous DNA and the efficiency of DNA integration in living cells. It is necessary to ascertain the fate of exogenous DNA for the development of nonviral gene therapy. This approach might also be extended to enhancement of iPS cell production using nonviral strategies because it has the potential to evaluate the stability of each plasmid factor in a target cell.

Acknowledgements

We thank Dr. K. Nemoto (Chibadai Inohana Innovation Plaza, Chiba, Japan) for technical help for CONTIN program. This work was partly supported by Grand-in-Aid for Scientific Research (A) 18207010 and (S) 21221006, by Grand-in-Aid for Exploratory Research (20657035) from JSPS, and No. 19058001 in Priority Area “Protein Community”.

Appendix A. Supplementary data

Supplementary data associated with this article can be found, in the online version, at doi:10.1016/j.jconrel.2009.12.013.

References

[1] C. Thomas, A. Ehrhardt, M. Kay, Progress and problems with the use of viral vectors for gene therapy, Nat. Rev., Genet. 4 (5) (2003) 346–358.
[2] K. Kaji, K. Norrby, A. Paca, M. Mileikovsky, P. Mohseni, K. Woltjen, Virus-free induction of pluripotency and subsequent excision of reprogramming factors, Nature 458 (7239) (2009) 771–775.
[3] D. Luo, W. Saltzman, Synthetic DNA delivery systems, Nat. Biotechnol. 18 (1) (2000) 33–37.
[4] J. Zabner, A. Fasbender, T. Moninger, K. Poellinger, M. Welsh, Cellular and molecular barriers to gene transfer by a cationic lipid, J. Biol. Chem. 270 (32) (1995) 18997–19007.
[5] A. Elouahabi, J. Ruysschaert, Formation and intracellular trafficking of lipoplexes and polyplexes, Molec. Ther. 11 (3) (2005) 336–347.
[6] A. Elouahabi, M. Thiry, V. Pector, J. Ruysschaert, M. Vandenbranden, Calorimetry of cationic liposome–DNA complex and intracellular visualization of the complexes, Methods Enzymol. 373 (2003) 313–332.
[7] Y. Zhang, L. Yu, Microinjection as a tool of mechanical delivery, Curr. Opin. Biotechnol. 19 (5) (2008) 506–510.
[8] E. Vaughan, D. Dean, Intracellular trafficking of plasmids during transfection is mediated by microtubules, Molec. Ther. 13 (2) (2006) 422–428.
[9] S. Somiari, J. Glasspool-Malone, J. Drabick, R. Gilbert, R. Heller, M. Jaroszeski, R. Malone, Theory and in vivo application of electroporative gene delivery, Molec. Ther. 2 (3) (2000) 178–187.
[10] E. Dauty, A. Verkman, Actin cytoskeleton as the principal determinant of size-dependent DNA mobility in cytoplasm: a new barrier for non-viral gene delivery, J. Biol. Chem. 280 (9) (2005) 7823–7828.
[11] G. Lukacs, P. Haggie, O. Seksek, D. Lechardeur, N. Freedman, A. Verkman, Size-dependent DNA mobility in cytoplasm and nucleus, J. Biol. Chem. 275 (3) (2000) 1625–1629.
[12] H. Pollard, G. Toumaniantz, J. Amos, H. Avet-Loiseau, G. Guihard, J. Behr, D. Escande, Ca2^{+}-sensitive cytosolic nucleases prevent efficient delivery to the nucleus of injected plasmids. J Gene Med 3(2) (2001) 153–164.
[13] D. Lechardeur, K. Sohn, M. Haardt, P. Joshi, M. Monck, R. Graham, B. Beatty, J. Squire, H. O'Brodovich, G. Lukacs, Metabolic instability of plasmid DNA in the cytosol: a potential barrier to gene transfer, Gene Ther. 6 (4) (1999) 482–497.
[14] T. Fisher, T. Terhorst, X. Cao, R. Wagner, Intracellular disposition and metabolism of fluorescently-labeled unmodified and modified oligonucleotides microinjected into mammalian cells, Nucleic Acids Res. 21 (16) (1993) 3857–3865.
[15] D. Lechardeur, A. Verkman, G. Lukacs, Intracellular routing of plasmid DNA during non-viral gene transfer, Adv. Drug Deliv. Rev. 57 (5) (2005) 755–767.
[16] M. Kinjo, R. Rigler, Ultrasensitive hybridization analysis using fluorescence correlation spectroscopy, Nucleic Acids Res. 23 (10) (1995) 1795–1799.
[17] J. Politz, E. Browne, D. Wolf, T. Pederson, Intranuclear diffusion and hybridization state of oligonucleotides measured by fluorescence correlation spectroscopy in living cells, Proc. Natl. Acad. Sci. U.S.A. 95 (11) (1998) 6043–6048.
[18] K. Remaut, B. Lucas, K. Raemdonck, K. Braeckmans, J. Demeester, S. De Smedt, Can we better understand the intracellular behavior of DNA nanoparticles by fluorescence correlation spectroscopy? J. Control. Release 121 (1–2) (2007) 49–63.
[19] K. Saito, I. Wada, M. Tamura, M. Kinjo, Direct detection of caspase-3 activation in single live cells by cross-correlation analysis, Biochem. Biophys. Res. Commun. 324 (2) (2004) 849–854.
[20] T. Takagi, H. Kii, M. Kinjo, DNA measurements by using fluorescence correlation spectroscopy and two-color fluorescence cross correlation spectroscopy, Curr. Pharm. Biotechnol. 5 (2) (2004) 199–204.
[21] R. Rigler, Z. Földes-Papp, F. Meyer-Almes, C. Sammet, M. Völcker, A. Schnetz, Fluorescence cross-correlation: a new concept for polymerase chain reaction, J. Biotechnol. 63 (2) (1998) 97–109.
[22] T. Ohrt, J. Mütze, W. Staroske, L. Weinmann, J. Höck, K. Crell, G. Meister, P. Schwille, Fluorescence correlation spectroscopy and fluorescence cross-correlation spectroscopy reveal the cytoplasmic origination of loaded nuclear RISC in vivo in human cells, Nucleic Acids Res. 36 (20) (2008) 6439–6449.
[23] S. Provencher, A constrained regularization method for inverting data represented by linear algebraic or integral equations, Comput. Phys. Commun. 27 (3) (1982) 213–227.
[24] S. Provencher, CONTIN — a general-purpose constrained regularization program for inverting noisy linear algebraic and integral equations, Comput. Phys. Commun. 27 (3) (1982) 229–242.

[25] S. Björling, M. Kinjo, Z. Földes-Papp, E. Hagman, P. Thyberg, R. Rigler, Fluorescence correlation spectroscopy of enzymatic DNA polymerization, Biochemistry 37 (37) (1998) 12971–12978.
[26] A. Pramanik, R. Rigler, Ligand–receptor interactions in the membrane of cultured cells monitored by fluorescence correlation spectroscopy, Biol. Chem. 382 (3) (2001) 371–378.
[27] E. Manders, H. Kimura, P. Cook, Direct imaging of DNA in living cells reveals the dynamics of chromosome formation, J. Cell Biol. 144 (5) (1999) 813–821.
[28] H. Nagaya, I. Wada, Y. Jia, H. Kanoh, Diacylglycerol kinase delta suppresses ER-to-Golgi traffic via its SAM and PH domains, Mol. Biol. Cell 13 (1) (2002) 302–316.
[29] M. Zanta, P. Belguise-Valladier, J. Behr, Gene delivery: a single nuclear localization signal peptide is sufficient to carry DNA to the cell nucleus, Proc. Natl. Acad. Sci. U.S.A. 96 (1) (1999) 91–96.
[30] M. van der Aa, G. Koning, J. van der Gugten, C. d'Oliveira, R. Oosting, W. Hennink, D. Crommelin, Covalent attachment of an NLS-peptide to linear DNA does not enhance transfection efficiency of cationic polymer based gene delivery systems, J. Control. Release 101 (1–3) (2005) 395–397.
[31] K. Hirata, M. Nishikawa, N. Kobayashi, Y. Takahashi, Y. Takakura, Design of PCR-amplified DNA fragments for in vivo gene delivery: size-dependency on stability and transgene expression, J. Pharm. Sci. 96 (9) (2007) 2251–2261.
[32] K. Ewert, H. Evans, A. Zidovska, N. Bouxsein, A. Ahmad, C. Safinya, A columnar phase of dendritic lipid-based cationic liposome–DNA complexes for gene delivery: hexagonally ordered cylindrical micelles embedded in a DNA honeycomb lattice, J. Am. Chem. Soc. 128 (12) (2006) 3998–4006.
[33] M. Santori, C. Gonzalez, L. Serrano, M. Isalan, Localized transfection with magnetic beads coated with PCR products and other nucleic acids, Nat. Protoc. 1 (2) (2006) 526–531.
[34] Y. Durocher, S. Perret, A. Kamen, High-level and high-throughput recombinant protein production by transient transfection of suspension-growing human 293-EBNA1 cells, Nucleic Acids Res. 30 (2) (2002) E9.
[35] S. Witko, C. Kotash, R. Nowak, J. Johnson, L. Boutilier, K. Melville, S. Heron, D. Clarke, A. Abramovitz, R. Hendry, M. Sidhu, S. Udem, C. Parks, An efficient helper-virus-free method for rescue of recombinant paramyxoviruses and rhadoviruses from a cell line suitable for vaccine development, J. Virol. Methods 135 (1) (2006) 91–101.
[36] J. Alwine, Transient gene expression control: effects of transfected DNA stability and trans-activation by viral early proteins, Mol. Cell. Biol. 5 (5) (1985) 1034–1042.
[37] K. Dörre, S. Brakmann, M. Brinkmeier, K. Han, K. Riebeseel, P. Schwille, J. Stephan, T. Wetzel, M. Lapczyna, M. Stuke, R. Bader, M. Hinz, H. Seliger, J. Holm, M. Eigen, R. Rigler, Techniques for single molecule sequencing, Bioimaging 5 (3) (1997) 139–152.